IET Microwaves, Antennas & Propagation

Research Article

IET Journals
The Institution of Engineering and Technology

UWB dual-polarised dipole array with dielectric and FSS superstrate and 65° scanning

ISSN 1751-8725
Received on 23rd January 2018
Revised 19th September 2018
Accepted on 25th October 2018
E-First on 28th January 2019
doi: 10.1049/iet-map.2018.5626
www.ietdl.org

Ersin Yetisir[1,2], Jiantong Li[1], Nima Ghalichechian[1] ✉

[1]*ElectroScience Laboratory, Department of Electrical and Computer Engineering, The Ohio State University, 1330 Kinnear Rd, Columbus, OH, USA*

[2]*SpaceX, 1 Rocket Rd, Hawthorne, CA, USA*

✉ *E-mail: ghalichechian.1@osu.edu*

Abstract: The authors report the design of an ultra-wideband (UWB), dual-polarised, tightly coupled dipole array (TCDA) with an integrated balun for wide-angle scanning. A dual-pol dipole design enables massive bandwidth, large scanning volume, and high polarisation purity, concurrently. To achieve wide-angle impedance matching without exciting surface waves, two types of superstrates are evaluated on a finite array: (i) dielectric superstrate and (ii) novel planar frequency-selective surface (FSS). The latter architecture is capable of scanning 70° in *E*-plane and 65° in *H*-plane and shows, on average, 5° scanning improvement to the former. The impedance bandwidth is 5.25:1 (0.8–4.2 GHz) at the broadside (voltage standing wave ratio (VSWR)<2). The bandwidth reduces to 4.3:1 (0.9–3.9 GHz) when the maximum scanning angle or θ_{max} increases to 65° for the *H*-plane and 70° for the *E*-plane (VSWR < 3.2). The proposed array is a great candidate for wide-angle wideband scanning applications covering the entire *L* and *S* bands.

1 Introduction

Ultra-wideband (UWB) antennas and arrays are essential for high data-rate communications, autonomous vehicles, and remote sensing. Novel approaches such as the advanced multifunction RF concept [1, 2] employ wideband apertures to reduce the number of antennas and RF/digital hardware for communication and radar applications. If wideband antenna arrays are capable of providing wide-angle scanning simultaneously with dual polarisation, they become significantly more attractive for a varied range of applications.

Tapered slot antennas, also known as *Vivaldi(s)*, are among the oldest and most popular wideband antenna elements [3–5]. Similarly, arrays of *Vivaldi* are attractive due to their large bandwidth and scan volume. Several variations of *Vivaldi* arrays have been reported to address bandwidth, modularity, power handling, and scanning [6–8]. However, since these arrays are typically formed by long vertically tapered conductors, they suffer from undesired radiation and reduced polarisation purity while scanning. Low-profile versions of Vivaldi antenna (e.g. balanced antipodal Vivaldi antenna or BAVA) have been shown to achieve better polarisation purity with impedance bandwidths up to 10:1 [9]. However, the BAVA architecture suffers from low efficiency while scanning, even for moderate scan angles (e.g. 45° from broadside).

Tightly coupled arrays are low-profile alternatives with high polarisation purity and excellent scanning [10]. Different designs with integrated feed focus on impedance bandwidth [11], modularity, and scalability [12]. However, most of these approaches are limited to <60° scan angle due to resistive losses [13] and surface waves [14].

In this paper, for the first time, we present a wideband dual-polarised tightly coupled dipole array (TCDA) that operates free of surface waves for scan angles up to 70°. A major challenge in designing dual-pol arrays (compared to single-pol) is maintaining low cross-polarisation (high polarisation purity or isolation) while preserving large bandwidth and scanning volume. This is quite challenging as the structure will have large overlaps with close proximity between feeding points with each linear polarisation. In summary, the proposed design exhibits the following unique features:

- Novel aperture design with overlapping dipoles providing dual-pol operation when compared with single-pol in the previous work [11, 15].
- The new design has the advantage of high polarisation purity when compared with our previous FSS-based single-pol designs [16, 17].
- Scanning capability of 65° in *E*- and *H*-planes when compared with <60° [18] with two linear polarisation. Specifically, superior scanning capability is 70° in *E*-plane.
- FSS planar superstrate layer using anisotropic material when compared with dielectric slab previously reported [19]. As a result, scanning performance is improved.
- A lossy and bulky Wilkinson power divider is removed in our design. The new architecture has the advantage of not using split unit cell of [19].
- Planar structure suitable for low-profile applications.
- Ultra-wide bandwidth covering 0.9–3.9 GHz (4.3:1).

The paper is organised as follows: Section 2 presents the geometry of the proposed design. Section 3 discusses coupling between feed lines and orthogonally polarised radiating elements which affect the overall bandwidth. Section 4 presents the full-wave simulation results, displaying the performance of the optimised array in terms of bandwidth, scanning, and polarisation isolation. In addition, a novel FSS superstrate is introduced in Section 5 showing improvement to the scanning performance. Finally, our conclusions are presented in Section 6.

2 Antenna geometry

The design of UWB and scanning arrays imposes several challenges. The bandwidth of connected dipole arrays significantly degrades when a backing reflector is used as a ground plane. This conductor acts as a shunt inductor at low frequencies. As the frequency declines, it dominates and shorts out the array causing impedance mismatch [20]. To mitigate the loading of ground at low frequencies, capacitive gaps are introduced between neighbouring dipoles along the *E*-plane. This capacitance compensates the inductive loading of the ground plane and provides better impedance matching, resulting in increased bandwidth. This is the

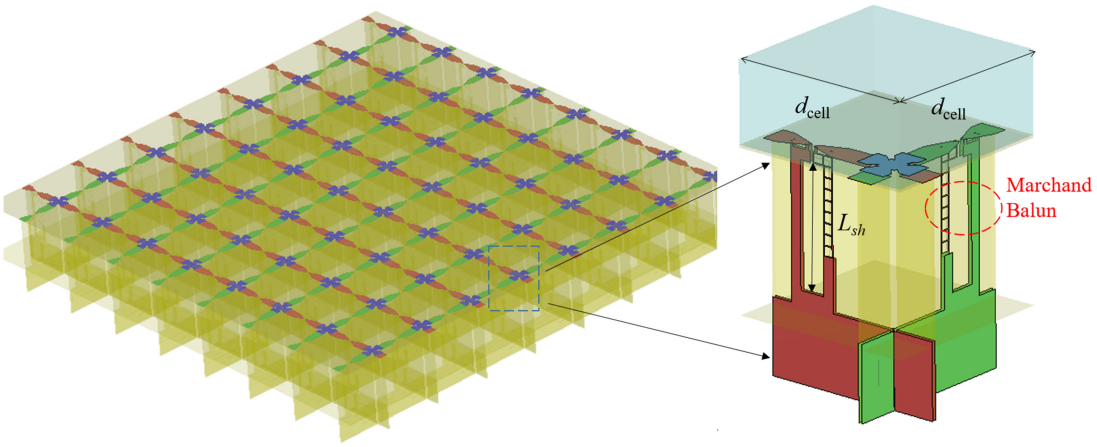

Fig. 1 *8 × 8 Dual-polarised TCDA (left) and its unit cell (right)*

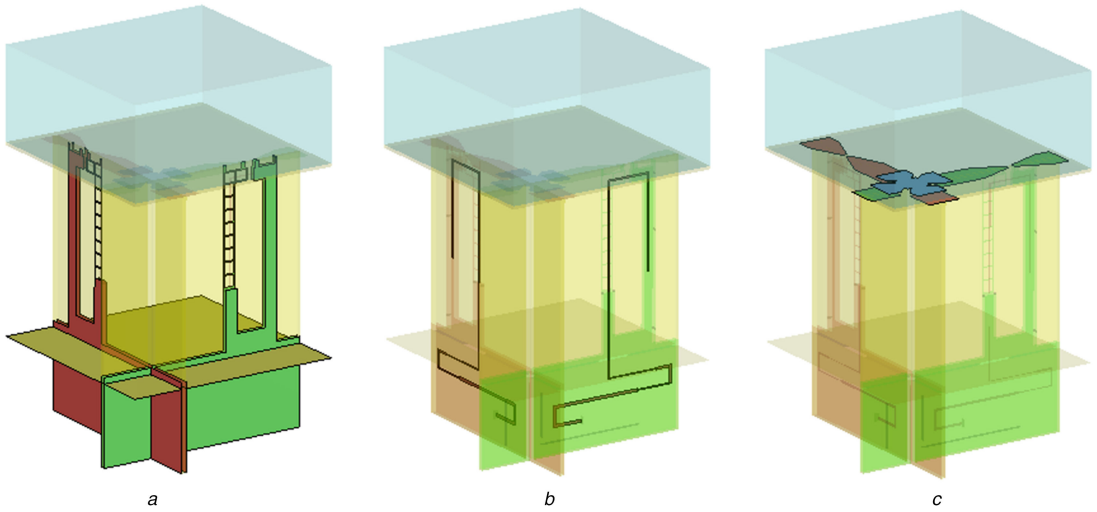

Fig. 2 *Major components of the unit cell of dual-polarised TCDA*
(a) Marchand balun (short stub), ***(b)*** Marchand balun (open stub), ***(c)*** Dipoles

main notion behind designing incredibly low-profile arrays by using capacitive coupling, as proposed by Munk *et al*. [10]. A major drawback of this approach is the need for a balanced feed (i.e. baluns) for the dipoles which adds to the total weight height, and volume of the antenna structure if external wideband baluns are used.

The dual-polarised 8 × 8 TCDA and the corresponding unit cell are shown in Fig. 1. The radiating dipoles are placed on a PCB (RO4003C laminate with $\varepsilon_r = 3.55$ and $\tan\delta = 0.0021$) with two copper layers, oriented parallel to the ground plane (shown in Fig. 2*a*). The thickness of the dielectric layer is 20 mil and detailed design of the overlapping dipoles is shown in Fig. 3. As shown here, two orthogonal dipoles form the horizontal and vertical polarisations. At the intersection of these two dipoles, however, the second metal layer is designed providing overlap and capacitive coupling between dipoles in each polarisation. This unique architecture provides UWB operation while maintains low cross-pol and large scanning volume.

Furthermore, the feeding structure is formed by a folded Marchand balun [21] implemented on two vertically oriented PCBs (RT/duroid 5880 laminate with $\varepsilon_r = 2.2$ and $\tan\delta = 0.001$) with three copper layers. The dielectric layer and bonding layer thickness are 29 and 4 mil, respectively. As seen in Fig. 4, portions of the Marchand balun are perforated with square slots resulting in an increase in the achievable characteristic impedance (Z_1) of the input line, in a manner similar to [16, 17]. In our first design, a low-permittivity dielectric slab (ECCOSTOCK-LoK with $\varepsilon_r = 1.7$ and $\tan\delta = 0.004$) was used as a superstrate to ensure a large scan range free of surface waves. The substrate of the array does not include a thick dielectric loading. This feature helped to increase the onset frequency of surface waves (out of the scan range and bandwidth of interest).

The proposed array was required to operate across 1–4 GHz with a minimum scan angle of 65° in the principle (*E* and *H*) planes. The design parameters were substrate and superstrate height (h_{sub}, h_{sup}), reactive loading of the shorted stub (W_{sh}, L_{sh}, H_{sh}), open stub (W_{op}, L_{op}), and the capacitive coupling (H_{couple}) between dipoles. We note that the dipole width (W_d) was not used in the optimisation loop. As is well known, wider dipoles provide better bandwidth, but degrade polarisation purity, especially while scanning. Therefore, we chose W_d as $0.15d_{cell}$, where d_{cell} is the size of the square-shape unit cell as shown in Figs. 1 and 3. Other parameters listed above are tuned to improve the impedance matching performance. The dielectric constant of the superstrate slab was kept constant during optimisation. The chosen material is a low-loss foam and can be used up to 10 GHz. These choices assure that the array can be fabricated with commercially available components at a reasonable cost. However, fabrication and testing of the array was not pursued in this work.

3 Reduction in cross-polarisation

In this section, the effects of coupling between cross-polarised elements and the resulting resonant common modes are discussed. Advanced Design Systems (Keysight Technologies) were used for initial design of the feed structure, ANSYS-HFSS was later on used for full-wave unit-cell simulation. In addition, 8 × 8 finite array simulation is using time-domain CST Design Studio. For simplicity, the input lines (Z_1–Z_5) inside the Marchand balun were removed and the array was simulated using 200 Ω gap sources, placed at the dipole inputs (see Fig. 3). The electrical current

density at common mode resonance frequency (f_{res} = 0.821 GHz) is compared to a non-resonant case (0.850 GHz) in Fig. 5. At resonance, high magnitudes of current are flowing through both active and terminated dipoles and baluns as shown in Fig. 5*b*. On the non-resonant structure, current density is much weaker and mostly confined to the active element (Fig. 5*a*). This indicates the common mode resonance is due to the coupling between the orthogonal dipoles and feed lines.

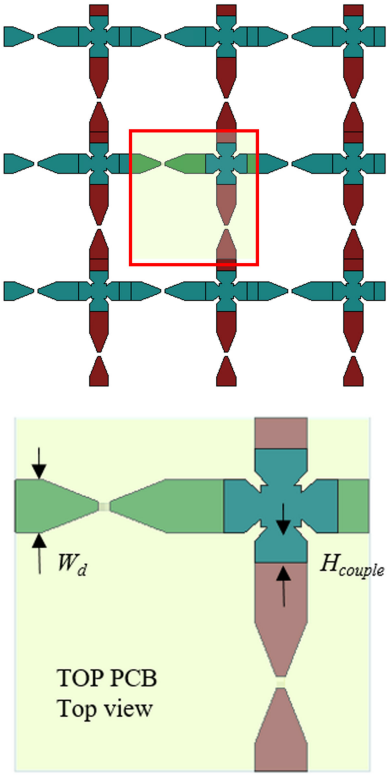

Fig. 3 *Top view of the unit cell containing the radiating elements with overlapping dipoles*

We acknowledge that even though the Marchand baluns were designed to provide differential current to the dipoles, they mostly carry common modes at f_{res}. These common mode currents on the active and passive baluns are in opposite directions. This indicates that the two orthogonally polarised dipoles with the baluns construct a resonating loop. Moreover, it verifies that the resonance is due to the coupling between cross-polarised dipoles and feeds.

To examine the parameters that affect f_{res}, we computed the port-to-port coupling (S_{12}) between the feeds of orthogonally polarised dipoles. This was done as a function of frequency and for different geometrical parameters: H_{sh}, L_{sh}, h_{sub} (see Figs. 1–4). For simplicity, the superstrate and the PCB substrates were removed during this parametric study. The resulting S_{12} data for L_{sh} = 2.5 cm, h_{sub} = 3.5 cm, H_{sh} = 0.7 cm, and d_{cell} = 3.45 cm (unless stated otherwise) is depicted in Fig. 6. From this figure, we observe that decreasing the balun width, H_{sh}, and increasing the ground plane height, h_{sub}, lowers f_{res}.

The shorted stub length, L_{sh}, has no significant effect on f_{res}. This observation further verifies that the resonating currents flow on the dipoles and through the outer edges of the baluns to form a loop, rather than passing through the shorted stub. Smaller frequency steps in Fig. 6 would actually indicate higher S_{12} values at the spikes. However, we were only interested at the value of f_{res} and not the exact magnitude of coupling. Using Ludwig's third definition [22], the far-field cross-polarisation purity around f_{res} is computed and depicted in Fig. 6*d*. We observe that the cross-polarised radiation can be as high as the co-polarisation (at 45° in *D*-plane). This is because, at the resonance, the radiating element is a loop formed by the orthogonal dipoles and the feed lines.

A similar loop resonance was reported in [12] due to unbalanced feeding of the crossed dipoles with via pins. As noted

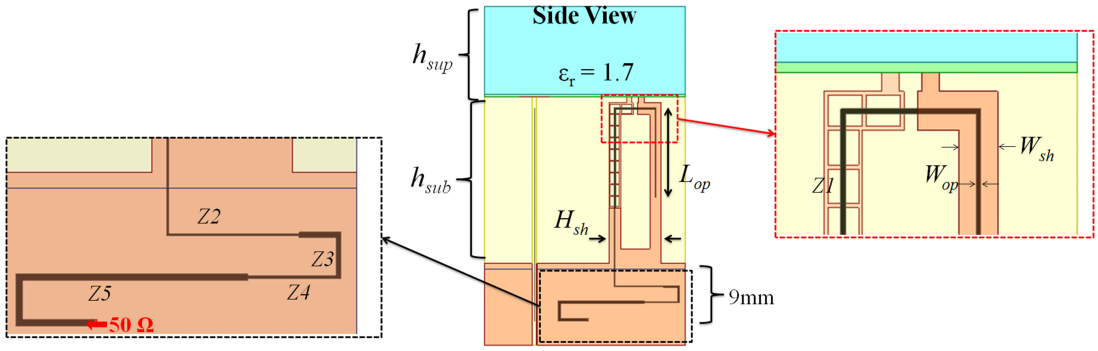

Fig. 4 *Detailed geometry of the feeding baluns and input lines with three copper layers. The input lines are formed by five-stage impedance transformer (Z_1, Z_2 ... Z_5). Z_1 is implemented as microstrip with perforated ground plane and Z_2–Z_5 is implemented as stripline*

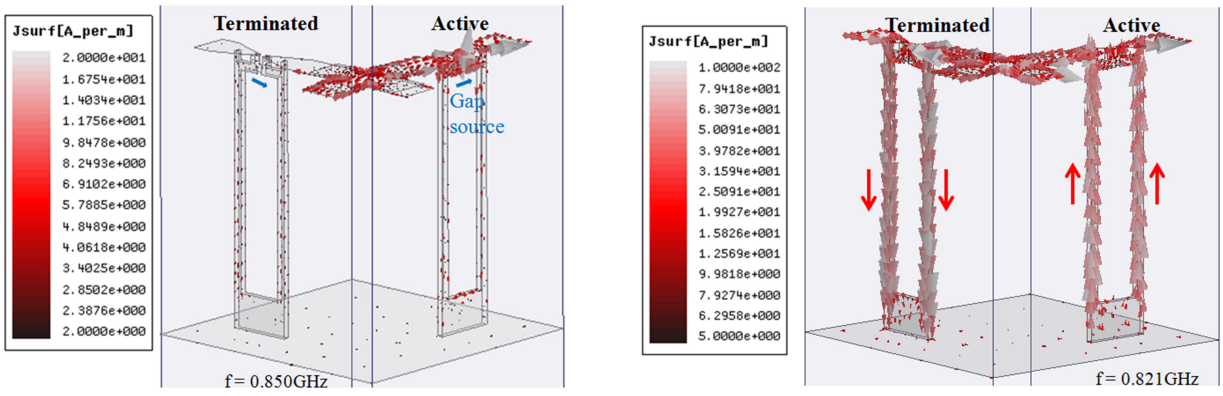

a *b*

Fig. 5 *Electrical current distribution inside the unit cell when only one polarisation is active*
(a) Current distribution at non-resonance, ***(b)*** Current distribution at common mode resonance

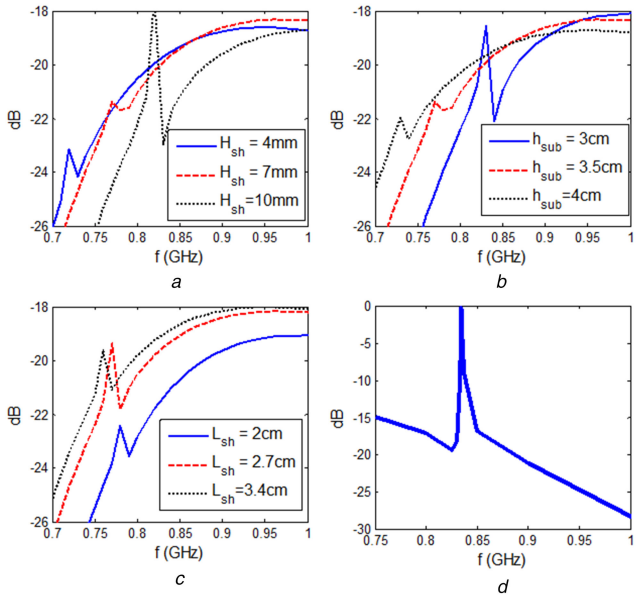

Fig. 6 *S_{12} versus frequency, as the unit-cell parameters are varied*

(a) S_{12} versus balun width, ***(b)*** S_{12} versus ground plane height, ***(c)*** S_{12} versus shorted stub length, ***(d)*** Normalised cross-polarised radiation for $h_{sub} = 3.5$ cm, $H_{sh} = 0.7$ cm, $L_{sh} = 2.3$ cm. The common mode resonances can be observed as sharp increases in S_{12} and cross-polarised radiation

Table 1 Optimised design parameters for unit cell

Parameter	Value	Parameter	Value	Parameter	Value
h_{sup}	15 mm	L_{op}	15 mm	Z_4	92 Ω
h_{sub}	30 mm	W_{op}	0.25 mm	Z_5	58 Ω
ε_r	1.7	W_d	5.2 mm	E_1	38°
L_{sh}	23 mm	H_{couple}	2 mm	E_2	39°
W_{sh}	2 mm	Z_1	140 Ω	E_3	9.4°
H_{sh}	9 mm	Z_2	98 Ω	E_4	9.9°
d_{cell}	35 mm	Z_3	64 Ω	E_5	40°

here, even balanced feeds (Marchand balun) cannot avoid this loop resonance. This is an important distinction that is typically not discussed in array designs. A loop resonance, despite using a high-quality differential feed, indicates that the excitation of this type of common mode is associated with the geometry of the unit cell rather than the quality of the individual feeding elements. As reported by Holland and Vouvakis [12], one can estimate the resonance frequency (f_{res}) of the common mode via the expression

$$f_{res} = \frac{c}{2\sqrt{\varepsilon_{eff}}\,(2d_{cell} + 4h_{sub} - H_{sh})} \quad (1)$$

Here, ε_{eff} represents the effective dielectric constant for the resonant path. Of course, ε_{eff} is close to unity when the substrate of the array is air. Equation (1) provides a simple way to approximate the resonance frequency and sets a limit at the low end of the operational bandwidth. We emphasise that the resonance frequency also depends on the coupling, H_{couple}, between dipoles. However, H_{couple} is a design parameter and not available at the beginning of optimisation process. Therefore, (1) should be used only as a coarse guide before optimisation of the array geometry.

4 Performance of the optimised array using dielectric superstrate

The array design parameters (W_{sh}, L_{sh}, H_{sh}, W_{op}, L_{op}, H_{couple}) were first optimised with ideal gap sources (200 Ω). Next, a five-stage impedance transformer was designed to match the 200 Ω input impedance of the balun down to 50 Ω of a standard connector placed below the ground plane. To do this, we employed a five-stage transmission line matching network as shown in Fig. 4. The impedance and electrical length of each stage are denoted by Z_i and E_i, respectively. Since the dipole input impedance is moderately high (200 Ω for wideband operation), for a practical stripline or microstrip, we perforated the ground plane of the transmission line for the first stage (Z_1, E_1). This approach is similar to [19] and makes it possible to fabricate a stripline with such high characteristic impedance ($Z_1 = 140$ Ω) without exceeding standard PCB fabrication limits (e.g. 4 mil minimum copper line width). Detailed design parameters of the finalised unit cell are provided in Table 1.

Assuming a standard 50 Ω source at the end of the five-stage transformer, simulated voltage standing wave ratio (VSWR) for different scan angles are plotted in Figs. 7 and 8, respectively. Fig. 7 shows that the bandwidth for broadside is 5.25:1 (0.8–4.2 GHz) in case that VSWR is <2, while the bandwidth is 0.9–4.1 GHz (VSWR<3) for 45° active scanning. As can be seen in Fig. 8, the array can scan to 65° along the *E*-plane and 60° along the *H*-plane with 0.9–3.9 GHz bandwidth (VSWR<3.2).

The port-to-port coupling between orthogonal elements is depicted in Fig. 9 when scanning along the *D*-plane. It is observed that the coupling is less than −17 and −10 dB for 45° and 60°, respectively. Furthermore, we chose *D*-plane as the port-to-port coupling is expected to be significantly larger than *E*- and *H*-planes. The normalised cross-polarised radiation is illustrated in Fig. 10 and is less than −20 and −17 dB for 45° and 60°, respectively. As well known for these type of dipole arrays, the cross-polarisation radiation and coupling performance is much better for the broadside and principle planes (less than −30 dB for our case). Therefore, when compared with the broadside and principle planes, only the *D*-plane results are shown in Figs. 9 and 10.

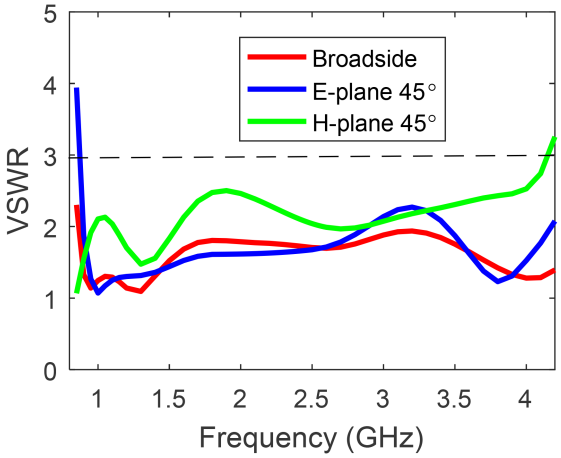

Fig. 7 *VSWR of the optimised array showing that θ = 45° for the principle planes covering the entire 0.8–4.2 GHz band*

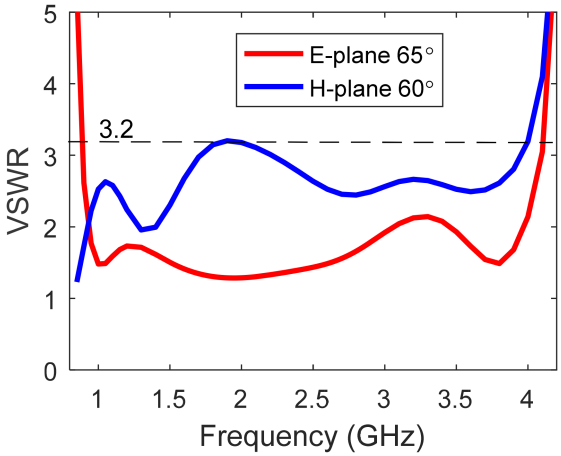

Fig. 8 *VSWR of the optimised array showing that θ = 60° for the principle planes covering the entire 0.9–3.9 GHz band*

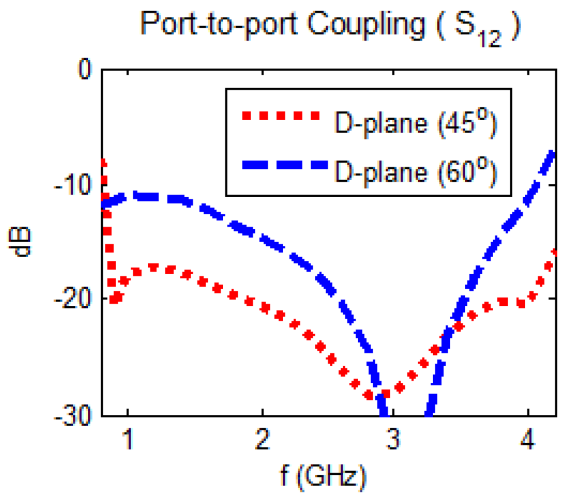

Fig. 9 *Coupling values between input ports of the orthogonally polarised dipoles when scanning in D-plane*

The simulated broadside realised gain is presented in Fig. 11. As can be seen, the simulated pattern agrees well with the theoretical gain calculation. Figs. 12 and 13 show the simulated *E*- and *H*-plane realised gain pattern at different frequencies from 1 to 4 GHz with step size of 1 GHz. The unit-cell size is designed based on highest frequency; therefore, the finite array can scan up to a limited angle. As expected, at the lower end of the band, the 8 × 8 array is electrically small. While the maximum scanning angle is determined at the highest frequency, as can be seen at 4 GHz, the maximum scanning angle is 65° at *E*-plane and 60° at *H*-plane. It is observed that the first sidelobe has the magnitude of −12 dB with respect to broadside beam.

5 Performance of the optimised array using FSS superstrate

For the array proposed in Section 4, the overall impedance bandwidth is 4.3:1 (0.9–3.9 GHz) when using 60° as scanning volume. As discussed in Section 3, the lower frequency limit is determined by the loop resonance. The upper limit is simply set by the electrical size of the unit cell which is 35 mm or 0.47λ at 4 GHz (highest frequency). The highest frequency (4 GHz) of operation is slightly smaller than the grating lobe frequency (4.4 GHz for 70°). The reason is that the higher order modes begin to dominate near the grating lobe frequency and it becomes quite difficult to

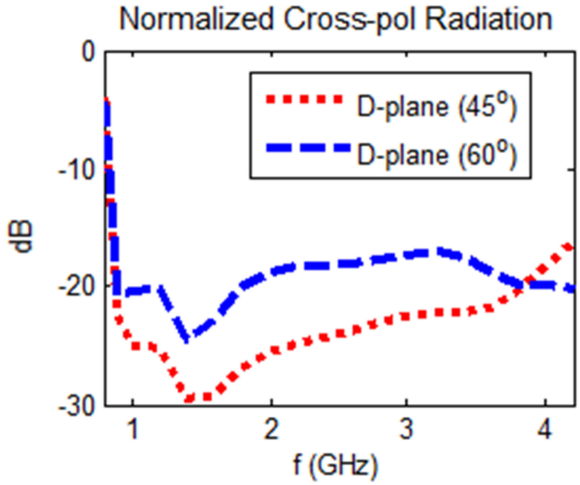

Fig. 10 *Cross-polarisation radiation based on Ludwig's third definition for orthogonally polarised dipoles when scanning in D-plane*

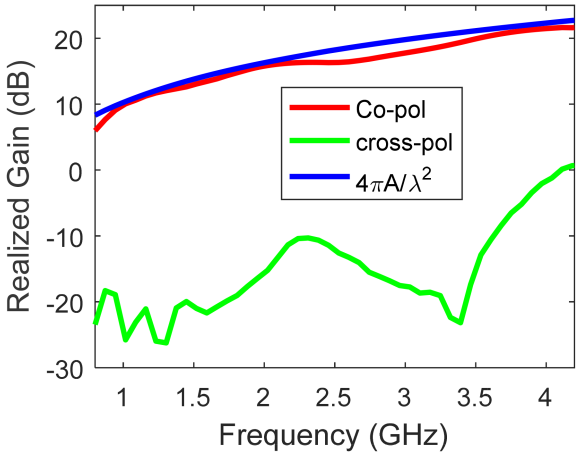

Fig. 11 *Broadside realised gain of the 8 × 8 antenna array showing that simulation agree well with the theoretical calculation*

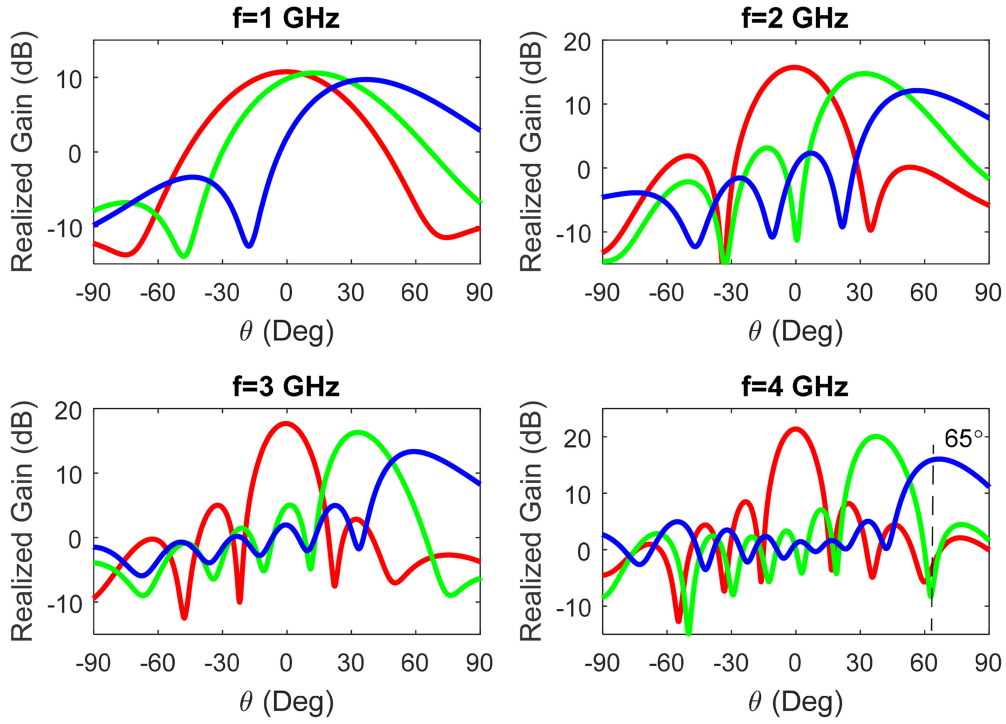

Fig. 12 *Realised gain patterns along the E-plane for the 8 × 8 array showing that the maximum scanning angle is 65° (four frequencies are illustrated). The adjacent array elements are phased for scanning angles of 0°, 30°, and 65°*

simultaneously impedance match the array across the entire scan range of interest.

To improve scanning volume, an FSS superstrate is used, as shown in Fig. 13. Unlike dielectric superstrate, FSS superstrate is

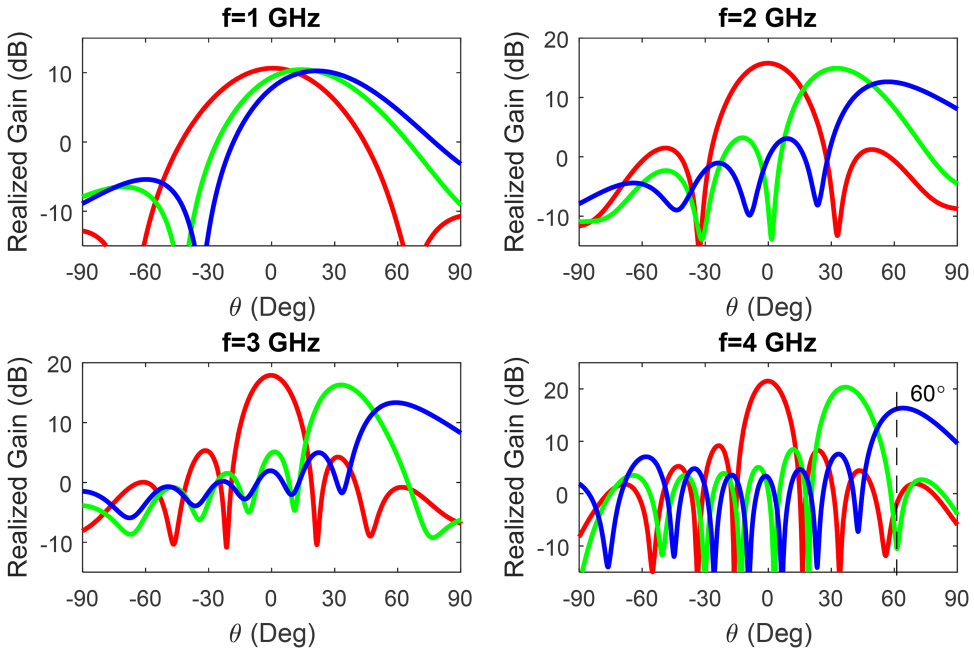

Fig. 13 *Realised gain patterns along the H-plane for the 8 × 8 array showing that the maximum scanning angle is 60° (four frequencies are illustrated). The adjacent array elements are phased for scanning angles of 0°, 30°, and 60°*

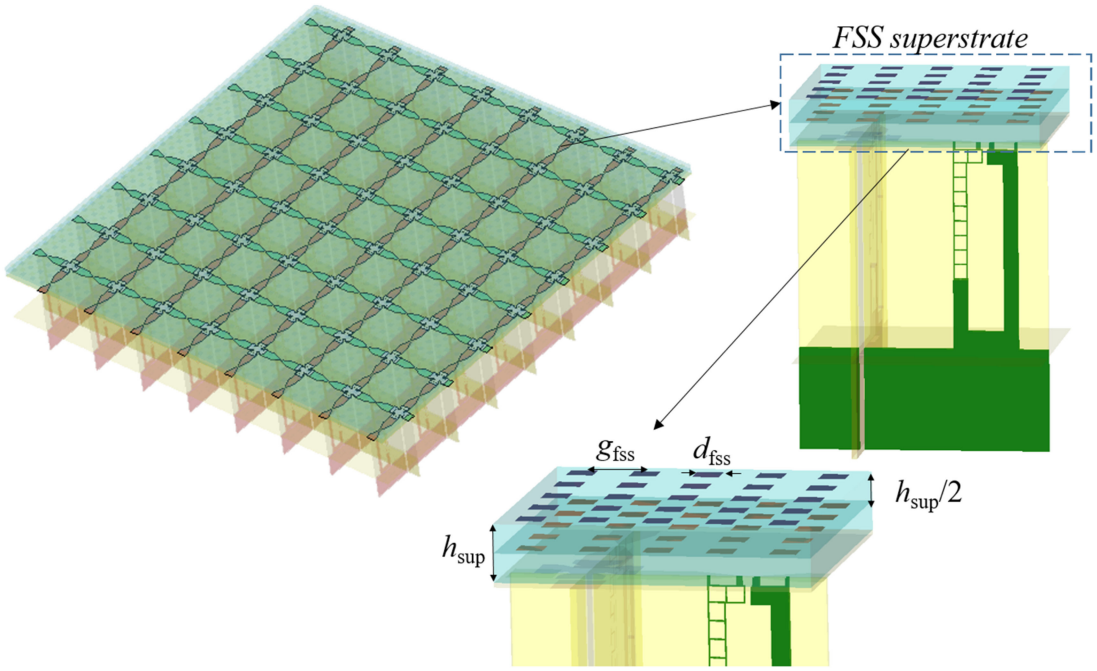

Fig. 14 *8 × 8 Dual-polarised TCDA using FSS superstrate(left) and its unit cell (right)*

anisotropic with different response to TE and TM waves. As can been seen, it consists of two PCB layers (RT/duroid 5880 laminate with $\varepsilon_r = 2.2$ and $\tan\delta = 0.001$) and 5 × 5 embedded patch elements. The dielectric layer and bonding layer thickness are 125 and 10 mil, respectively. The variables are d_{fss} for patch size, g_{fss} for element spacing, and h_{sup} for superstrate height (shown in Fig. 14). To satisfy impedance matching for *E*- and *H*-plane scanning, the specific values are: $d_{fss} = 3.5$ mm, $g_{fss} = 7.5$ mm, and $h_{sup} = 7.375$ mm.

As can be seen from Fig. 15, the array with FSS superstrate can scan up to 70° along the *E*-plane and 65° along the *H*-plane with 0.9–3.9 GHz bandwidth (VSWR<3.2). Figs. 16 and 17 show the simulated *E*- and *H*-plane realised gain pattern at different frequencies from 1 to 4 GHz with 1 GHz as step size. In comparison with dielectric superstrate, it is improved from 65° to 70° at *E*-plane, from 60° to 65° at *H*-plane. This improvement is the result of anisotropic dielectric behaviour of the FSS. We note that we are operating FSS at frequency well below its resonance frequency (i.e. acting as a capacitive layer). As can be seen, the first sidelobe has the magnitude of −12 dB compared to broadside beam. Consequently, the proposed 8 × 8 array using FSS superstrate can provide 0.9–3.9 GHz bandwidth with VSWR<3.2 when scanning 70° at *E*-plane, 65° at *H*-plane.

6 Discussion and conclusions

In this paper, we presented two versions of UWB dual-polarised TCDAs with large scanning volume. For a dual-pol antenna, impedance bandwidth limitation is due to coupling between the orthogonal elements, resulting in a low-frequency resonance [12]. To suppress the modes of this resonance, we examined port-to-port coupling by optimising the design parameters of superstrate height, reactive loading, and capacitive coupling.

For the first design, dielectric superstrate was used to enhance the scanning volume free of surface waves. The impedance

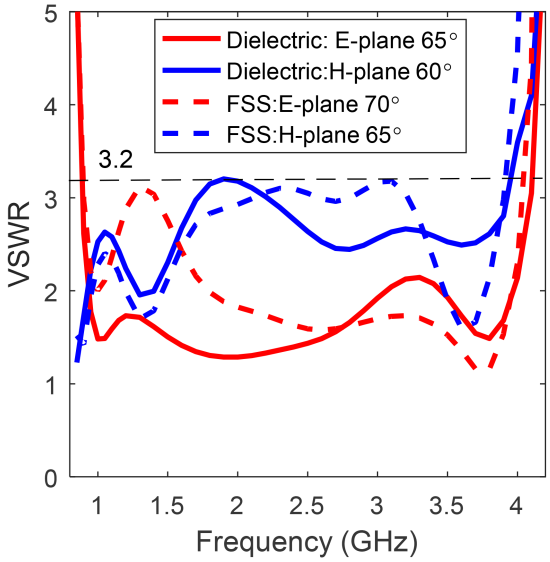

Fig. 15 *VSWR of the optimised array using dielectric superstrate and FSS superstrate showing that FSS superstrate improves 5° for the principle planes covering the entire 0.9–3.9 GHz band*

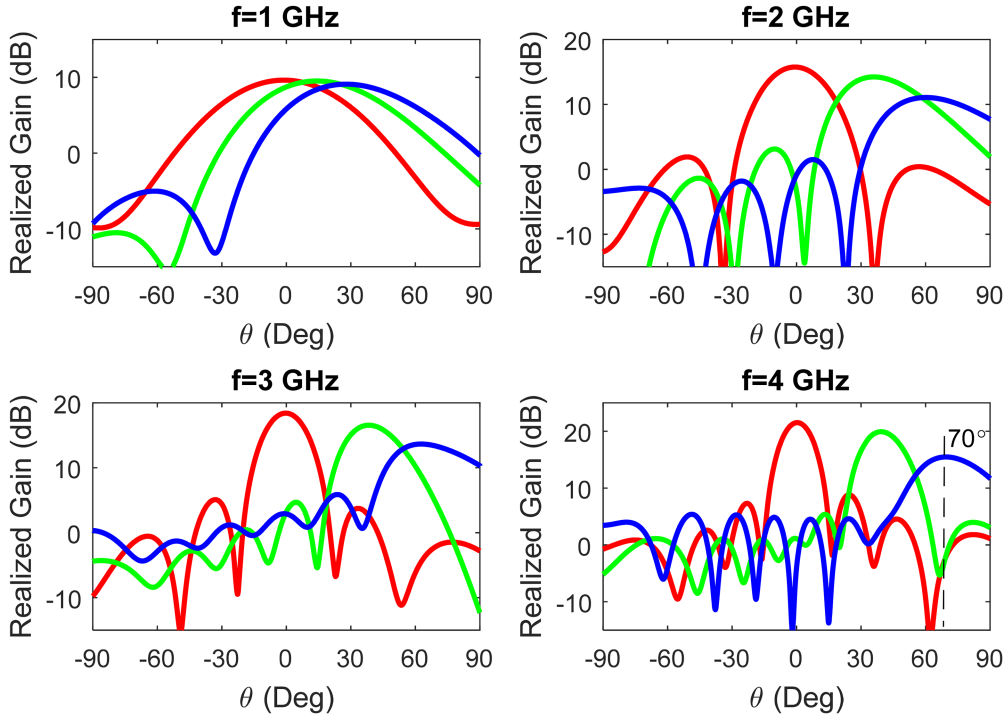

Fig. 16 *Realised gain patterns along the E-plane for the 8 × 8 array showing that the maximum scanning angle is 70° (four frequencies are illustrated). The adjacent array elements are phased for scanning angles of 0°, 30°, and 70°*

bandwidth (VSWR < 2) for broadside was 5.25:1 but was reduced to 4.3:1 when scanning to 60°. The maximum scan angles were 60° for *H*-plane and 65° for *E*-plane.

In order to achieve a larger scanning volume, the novel planar FSS superstrate was designed to push surface waves to higher frequency. Compared with dielectric superstrate, the FSS superstrate acted as an anisotropic and extra matching layer that enhanced scanning. Consequently, the maximum scanning angles were 65° for *H*-plane and 70° for *E*-plane. The impedance bandwidth (VSWR < 3.2) was 4.3:1 when scanning to 65°. Therefore, the FSS superstrate improved the scanning by 5° when compared with the dielectric superstrate. We note that this improvement is the result of FSS anisotropic dielectric layer operating below its resonance frequency.

To improve bandwidth at the lower frequency end, a feeding structure/balun with a smaller footprint (H_{sh}) can be used, as suggested by Fig. 6*a* results. Another option is to use dielectric loading in the substrate layer of the array. This can increase the electrical length of the resonant path, and therefore, decrease the common mode frequency. Consequently, wider bandwidth can be achieved. However, a thicker substrate would also result in a thick dielectric slab ($h_{sub} + h_{sup}$) over the ground plane, causing earlier onset of surface waves and limiting the scan range. For bandwidth improvement at the higher frequency bands, the height of the superstrate material can be reduced. This way, the onset of surface waves can be pushed to higher frequencies and larger scan angles. Since we already achieved the required bandwidth and scan range, we did not pursue these improvements.

The designed FSS array achieved wide scanning impedance match without excitation of surface waves. The latter design was capable of scanning 70° in *E*-plane and 65° in *H*-plane, showing 5° scanning improvement to dielectric superstrate. In addition, the impedance bandwidth was 5:25:1 (0.8–4.2 GHz) at the broadside (VSWR<2) and it was reduced to 4.3:1 (0.9–3.9 GHz) for the maximum scanning angle (VSWR<3.2). Although, achieved at the expense of a more complex superstrate structure, the FSS

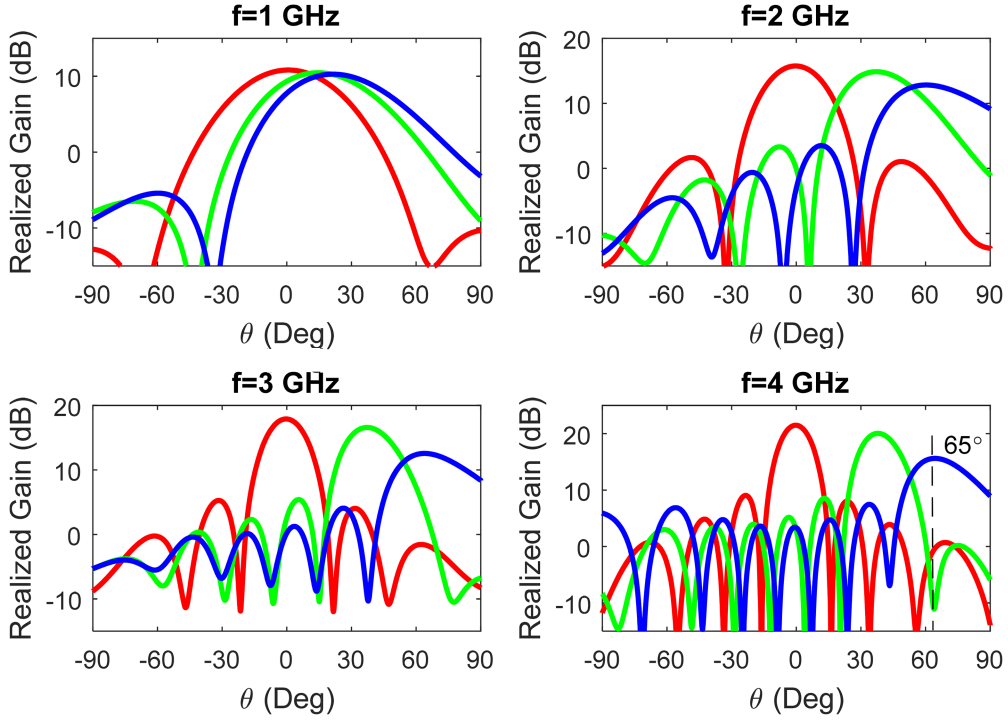

Fig. 17 *Realised gain patterns along the H-plane for the 8 × 8 array showing that the maximum scanning angle is 65° (four frequencies are illustrated). The adjacent array elements are phased for scanning angles of 0°, 30°, and 65°*

superstrate and antenna array can be simultaneously fabricated using PCB technology.

For validation of the design, we have previously shown in [16, 17] that the measured patterns have a good agreement with full-wave simulation of a *finite* array. Although fabrication and measurement was not the scope of this work, simulated pattern of the finite array presented in Figs. 12, 13, 16, and 17 serve as an initial verification and proof of concept.

7 Acknowledgments

The authors would like to acknowledge Mr Loc Chau from Northrop Grumman Aerospace Systems for his input and assistance with this project. We would also like to thank Northrop Grumman Aerospace Systems and DARPA, as well as Dr Troy Olsson for their support. We would also like to thank Professor John Volakis from Florida International University for his suggestions and discussions.

8 References

[1] Tavik, G.C., Hilterbrick, C.L., Evins, J.B., *et al.*: 'The advanced multifunction RF concept', *IEEE Trans. Microw. Theory Tech.*, 2005, **53**, (3), pp. 1009–1020

[2] Hughes, P.K., Choe, J.Y.: 'Overview of advanced multifunction RF system (AMRFS)'. Proc. 2000 IEEE Int. Conf. on Phased Array Systems and Technology, 2000, pp. 21–24

[3] Gibson, P.J.: 'The Vivaldi aerial'. 9th European Microwave Conf., 1979, pp. 101–105

[4] Gazit, E.: 'Improved design of the Vivaldi antenna', *IEE Proc. H – Microwav., Antennas Propag.*, 1988, **135**, (2), pp. 89–92

[5] Langley, J.D.S., Hall, P.S., Newham, P.: 'Novel ultrawide-bandwidth Vivaldi antenna with low crosspolarisation', *Electron. Lett.*, 1993, **29**, (23), pp. 2004–2005

[6] Holter, H.: 'Dual-polarized broadband array antenna with BOR-elements, mechanical design and measurements', *IEEE Trans. Antennas Propag.*, 2007, **55**, (2), pp. 305–312

[7] Schaubert, D.H., Kasturi, S., Boryssenko, A.O., *et al.*: 'Vivaldi antenna arrays for wide bandwidth and electronic scanning'. The Second European Conf. on Antennas and Propagation, EuCAP, Edinburgh, UK, November 2007, pp. 1–6

[8] Kindt, R.W., Pickles, W.R.: 'Ultrawideband all-metal flared-notch array radiator', *IEEE Trans. Antennas Propag.*, 2010, **58**, (11), pp. 3568–3575

[9] Elsallal, M.W., Mather, J.C.: 'An ultra-thin, decade (10:1)) bandwidth, modular BAVA array with low cross-polarization'. 2011 IEEE Int. Symp. on Antennas and Propagation (APSURSI), 2011, pp. 1980–1983

[10] Munk, B., Taylor, R., Durbam, T., *et al.*: 'A low-profile broadband phased array antenna'. IEEE Antennas and Propagation Society Int. Symp., USNC/CNC/URSI North American Radio Sci. Meeting, Columbus, OH, USA, June 2003, vol. 2, pp. 448–451

[11] Doane, J.P., Sertel, K., Volakis, J.L.: 'A wideband, wide scanning tightly coupled dipole array with integrated balun (TCDA-IB) (in English)', *IEEE Trans. Antennas Propag.*, 2013, **61**, (9), pp. 4538–4548

[12] Holland, S.S., Vouvakis, M.N.: 'The planar ultrawideband modular antenna (PUMA) array', *IEEE Trans. Antennas Propag.*, 2012, **60**, (1), pp. 130–140

[13] Moulder, W.F., Sertel, K., Volakis, J.L.: 'Superstrate-enhanced ultrawideband tightly coupled array with resistive FSS', *IEEE Trans. Antennas Propag.*, 2012, **60**, (9), pp. 4166–4172

[14] Pozar, D., Schaubert, D.: 'Scan blindness in infinite phased arrays of printed dipoles', *IEEE Trans. Antennas Propag.*, 1984, **32**, (6), pp. 602–610

[15] Kasemodel, J.A., Chen, C.-C., Volakis, J.L.: 'Wideband planar array with integrated feed and matching network for wide-angle scanning', *IEEE Trans. Antennas Propag.*, 2013, **61**, (9), pp. 4528–4537

[16] Yetisir, E., Ghalichechian, N., Volakis, J.L.: 'Ultrawideband array with 70 degree scanning using FSS superstrate', *IEEE Trans. Antennas Propag.*, 2016, **64**, (10), pp. 4256–4265

[17] Yetisir, E., Ghalichechian, N., Volakis, J.L.: 'Wideband & wide angle scanning array with parasitic superstrate'. 2015 IEEE International Symposium on Antennas and Propagation & USNC/URSI National Radio Science Meeting, Vancouver, BC, Canada, July 2015, pp. 2521–2522

[18] Zhang, H., Yang, S., Chen, Y., *et al.*: 'Wideband dual-polarized linear array of tightly coupled elements', *IEEE Trans. Antennas Propag.*, 2018, **66**, (1), pp. 476–480

[19] Novak, M.H., Volakis, J.L.: 'Ultrawideband antennas for multiband satellite communications at UHF–Ku frequencies', *IEEE Trans. Antennas Propag.*, 2015, **63**, (4), pp. 1334–1341

[20] Munk, B.: 'Broadband wire arrays', in '*Finite antenna arrays and FSS*' (Wiley-IEEE Press, Hoboken, NJ, USA, 2003), pp. 181–213

[21] Marchand, N.: 'Transmission-line conversion transformers', *Electronics (Basel)*, 1944, **17**, (12), pp. 142–145

[22] Ludwig, A.: 'The definition of cross polarization', *IEEE Trans. Antennas Propag.*, 1973, **21**, (1), pp. 116–119